LAWRENCE
LIVERMORE
NATIONAL
LABORATORY

LLNL-JRNL-569456

Global Sampling for Integrating Physics-Specific Subsystems and Quantifying Uncertainties of CO2 Geological Sequestration

Y. Sun, C. Tong, W. J. Trainor-Guitten, C. Lu, K. Mansoor, S. A. Carroll

August 3, 2012

International Journal of Greenhouse Gas Control

Disclaimer

Global Sampling for Integrating Physics-Specific Subsystems and Quantifying Uncertainties of CO_2 Geological Sequestration

Y. Sun[1], C. Tong, W.J. Trainor-Guitton, C. Lu, K. Mansoor, S.A. Carroll
Lawrence Livermore National Laboratory, Livermore, CA 94551

ABSTRACT

The risk of CO_2 leakage from a deep storage reservoir into a shallow aquifer through a fault is assessed and studied using physics-specific computer models. The hypothetical CO_2 geological sequestration system is composed of three subsystems: a deep storage reservoir, a fault in caprock, and a shallow aquifer, which are modeled respectively by considering sub-domain-specific physics. Supercritical CO_2 is injected into the reservoir subsystem with uncertain permeabilities of reservoir, caprock, and aquifer, uncertain fault location, and injection rate (as a decision variable). The simulated pressure and CO_2/brine saturation are connected to the fault-leakage model as a boundary condition. CO_2 and brine fluxes from the fault-leakage model at the fault outlet are then imposed in the aquifer model as a source term. Uncertainties are propagated from the deep reservoir model, to the fault-leakage model, and eventually to the geochemical model in the shallow aquifer, thus contributing to risk profiles. To quantify the uncertainties and assess leakage-relevant risk, we propose a global sampling-based method to allocate sub-dimensions of uncertain parameters to sub-models. The risk profiles are defined and related to CO_2 plume development for pH value and total dissolved solids (TDS) below the EPA's Maximum Contaminant Levels (MCL) for drinking water quality. A global sensitivity analysis is conducted to select the most sensitive parameters to the risk profiles. The uncertainty of pH- and TDS-defined aquifer volume, which is impacted by CO_2 and brine leakage, mainly results from the uncertainty of fault permeability. Subsequently, high-resolution, reduced-order models of risk profiles are developed as functions of all the decision variables and uncertain parameters in all three subsystems.

Keywords: Uncertainty quantification; CO_2 sequestration; risk assessment; reactive transport; global sampling.

1. Introduction

Geological sequestration of CO_2 results in pressure build-up and geomechanical alternation in the storage reservoir. This increases the probability of re-activation of faults in the caprock seal, and further elevates the risk of CO_2 and brine leakage into drinking-water resources (Gasda et al., 2004; Bachu, 2008; Celia et al., 2008; Carroll et al., 2009; Apps et al., 2010; Pruess, 2011; Siirila et al., 2012). Migration of CO_2 and brine towards a shallow aquifer through various leakage pathways, such as abandoned wellbores, faults, and fracture networks, is the primary concern for decreasing groundwater pH and an increasing concentration of total dissolved solids (Carroll et al., 2009; Siirila et al., 2012), because the decreased pH alters reaction chemistry and may lead to elevated concentrations of primary contaminants and the increased TDS may yield an undrinkable water.

[1]Corresponding author: Lawrence Livermore National Laboratory, 7000 East Avenue, Livermore, CA 94551; (925) 422-1587; fax (925) 423-0153; sun4@llnl.gov

As a result of rapid advances in numerical methods for modeling multi-phase reactive transport and the availability of high-performance computers, physics-based process modeling has been widely used to address pressure buildup, storage capacity, injectivity, CO_2-rock interactions, leakage pathways, and risks (Siirila et al., 2012). In the presence of various sources of uncertainties, such as conceptual model uncertainties (including geological-structure uncertainties), model parameter uncertainties, experimental- and field-data uncertainties, there is a need to develop a rigorous and integrated framework for quantifying the relationship between the uncertainty of ultimate risk profiles and all input uncertainties from various physics-specific subsystems (Tartakovsky et al., 2011).

The risk assessment of a geological sequestration system includes various components, such as reservoir management, evaluation of wellbore and caprock integrity, ensuring the protection of groundwater, and identification of geochemical impact on groundwater (Guthrie, 2009). Reservoir, fault- and wellbore-leakage, and geochemical subsystems have been mostly modeled and studied separately (i.e., Zhou et al., 2008; Birkholzer et al., 2009; Viswanathan et al., 2008; Carroll et al., 2009; Jordan et al., 2011; Yang et al., 2011; Zhang et al., 2011; Buscheck et al., 2011, 2012). Rigorous uncertainty quantification of all sources in all subsystems and an overall risk assessment should be an integral process of the updated system simulation and decision-making in CO_2 geological sequestration. Subsystems may be simulated by physics-specific sub-models. Recently, Remoroza et al. (2011) and Pan et al. (2011) coupled wellbore and reservoir models to address the injection-dependent CO_2 leakage. To integrate various sub-model results for uncertainty quantification and risk assessment of CO_2 geological sequestration, scientists at Los Almos National Laboratory developed CO_2-PENS (Viswanathan et al., 2008; Stauffer et al., 2009; Jordan et al., 2011).

Uncertainties of a geologic system may result from the geologic structure and system parameters (Dai et al., 2007; Liu and Zhang, 2011; Keating et al., 2011; Refsgaard et al., 2011). The uncertainty of geologic structure and physical processes is also called conceptual-model uncertainty. Traditionally, deterministic models of reactive transport in the subsurface are developed on a single, but presumably known geologic structure with uncertain system properties (Clement et al., 1998; 2000; Sun et al., 2010; 2012b). Uncertainties of conceptual models and system parameters have not been rigorously studied together as an integral part for risk assessment of CO_2 geological sequestration.

In this paper, we present a global sampling method to allocate sub-dimensions of uncertain inputs to physics-specific sub-models and to quantify the uncertainty of the ultimate outputs, such as the risk profiles defined as aquifer volume affected by CO_2 and brine leakage. Sample points are generated to sufficiently cover the high-dimensional space of uncertainties. While partial dimensions are used to describe heterogeneous aquifer structure and fault location, others are used to reflect the variation of system parameters. Finally, the risk profiles, relevant to CO_2 and brine leakage, are assessed as functions of uncertain parameters and decision variables.

2. Model Development and Solution Method

In this study, we focus on a geological sequestration system, which is composed of a hypothetical storage reservoir, a hypothetical fault, and a shallow groundwater system to represent the High Plains aquifer. As shown in Figure 1, a vertical fault cuts through the overburden caprock and connects the reservoir and the shallow aquifer. Three process models are developed to represent reservoir (RS), fault (FT), and aquifer (AQ) subsystems respectively. Hereby, we use *aquifer* and *reservoir* to represent the shallow groundwater formation and the deep saline formation for CO_2 storage, respectively.

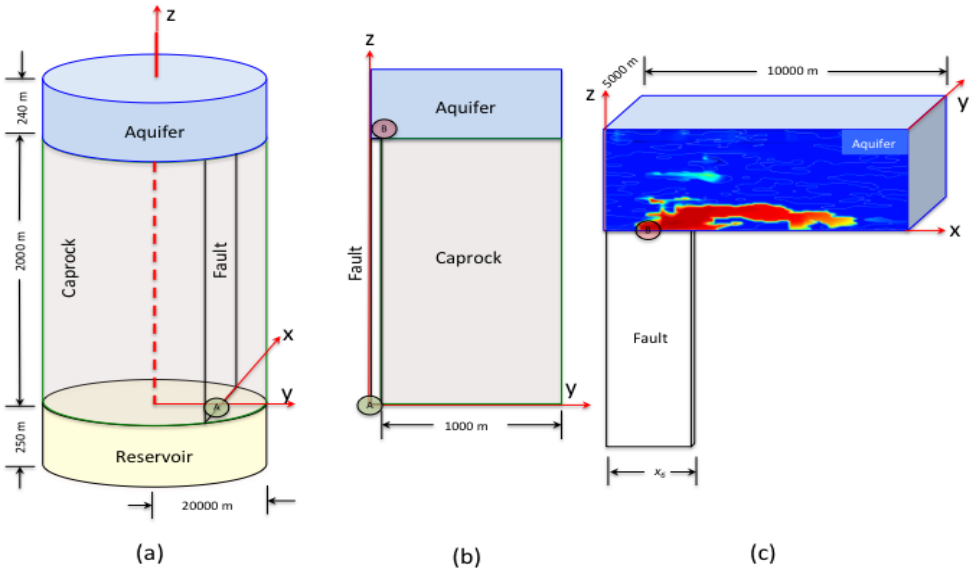

Figure 1. Conceptual models. (a) Radially-symmetric reservoir model (RS), (b) Two-dimensional fault leakage model (FT), and (c) Three-dimensional aquifer model (AQ).

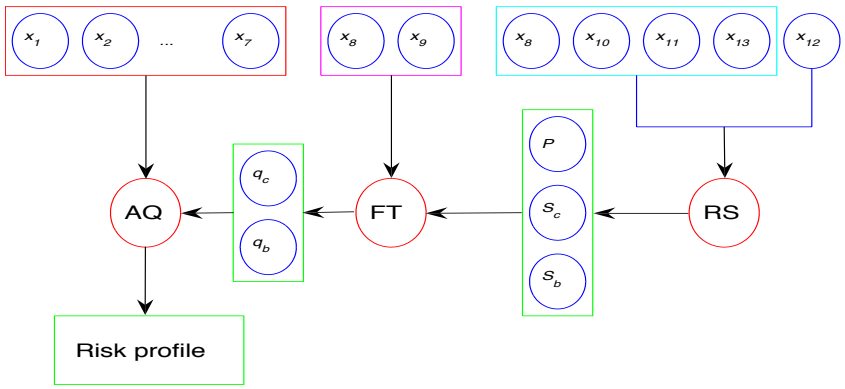

Figure 2. Flow chart of global sampling method of process modeling. Permeabilities of caprock, reservoir, and lumped aquifer (x_8, x_{10}, x_{13}), injection rate (x_{11}), and fault distance from injection center (x_{12}), are uncertain inputs to reservoir subsystem (RS). Probabilistic outputs, pressure (P) and CO_2 and brine saturation (S_c, S_b), and permeabilities of caprock and fault (x_8, x_9), are uncertain inputs to fault-leakage subsystem (FT). CO_2 and brine fluxes (q_c, q_b), heterogeneity-relevant parameters (x_1, x_2, and x_3), permeabilities of sand and clay in aquifer (x_4, x_5), longitudinal fault length (x_6), and brine molality (x_7), are uncertain inputs to the aquifer subsystem (AQ).

Table 1. Uncertain parameters and intervals.

Symbol	Parameter	Minimum	Maximum	Unit
x_1	Sand volume fraction of *aquifer*	0.35	0.65	[-]
x_2	Correlation length of clay in x	200.0	2500.0	[m]
x_3	Correlation length of clay in z	0.5	25.0	[m]
x_4	Sand permeability of *aquifer*	-13.0	-10.0	$\log_{10}[m^2]$
x_5	Clay permeability of *aquifer*	-18.0	-15.0	$\log_{10}[m^2]$
x_6	Fault length in x	100.0	1000.0	[m]
x_7	Brine molality	0.3	3.0	[mol kg^{-1}]
x_8	Permeability of caprock	-21.0	-16.0	$\log_{10}[m^2]$
x_9	Permeability of fault	-16.0	-13.0	$\log_{10}[m^2]$
x_{10}	Permeability of *reservoir*	-14.0	-11.0	$\log_{10}[m^2]$
x_{11}	Injection rate (decision variable)	50.0	100.0	[kg s^{-1}]
x_{12}	Distance between injection well and fault	100.0	1000.0	[m]
x_{13}	Lumped permeability of *aquifer*	$x_{13} = x_1x_4 + (1-x_1)x_5$		$\log_{10}[m^2]$

Uncertain parameters and their respective ranges needed to specify process models are listed in Table 1 and the input-output structure of three subsystems is shown in Figure 2. Ultimately, the risk profile, which is defined as aquifer volume affected by CO_2 and brine leakage, is generated as a function of uncertain parameters and decision variables. The permeability of the aquifer is calculated as a function of sand and clay permeabilities, and sand volume fraction as an intermediate parameter in RS models.

2.1. Reservoir Process Model (RS)

A two-dimensional radially symmetric model is used to represent two-phase (super-critical CO_2 and brine) flow, with temperature and pressure dependent density of supercritical-CO_2 (Span and Wagner, 1996), within a 250-m-thick saline storage formation, as modeled by Zhou et al. (2008) and Buscheck et al. (2012), with the top of the storage formation located 2240 m below ground surface and bounded by 2000-m-thick caprock. The outer-lateral and bottom boundaries are assumed to be impermeable for a no-flow condition (Figure 1a). A 240-m-thick aquifer with lumped physical properties is overlaid on the top caprock seal. The storage formation is assumed to be homogeneous and initially saturated with brine. Caprock permeability (x_8) (see Table 1), reservoir permeability (x_{10}), aquifer permeability (x_{13}), CO_2 injection rate (x_{11}), and the distance between injection field and the leaky fault (x_{12}), are five uncertain inputs considered in the reservoir model. Pressure and saturation profiles (of CO_2 and brine) at an uncertain location (Ⓐ in Figure 1a) (x_{12}) are the outputs from the reservoir model and inputs to fault-leakage model.

2.2. Fault-Leakage Process Model (FT)

The potential leakage of CO_2 and brine through a vertical fault from the saline formation to a shallow aquifer is simulated by a two-dimensional two-phase flow and thermal model (Sun et al., 2010) with temperature- and pressure-dependent CO_2 density and enthalpy (Span and Wagner, 1996; Lu et al., 2012), and phase transition. Permeabilities and capillary-pressure parameters of fault and caprock, and fault width, were initially believed to play major roles in buoyancy-driven flow. From the Sobol' sensitivity analysis (Sobol', 1990) of CO_2 and brine fluxes at the outlet of fault (Ⓑ in Figure 1b), we select permeabilities of fault and caprock, as well as pressure and saturation profiles simulated from the reservoir

model at the fault inlet, as uncertain inputs to fault-leakage model. Fluxes of CO_2 and brine at the fault outlet are outputs of fault leakage model and uncertain inputs to the aquifer model. It is assumed that both CO_2 and brine fluxes are so small that they do not cause a pressure release in the reservoir subsystem. The pressure release from the reservoir model is not simulated.

2.3. Aquifer Process Model (AQ)

A three-dimensional High Plains aquifer consisting of sand and clay (Carroll et al., 2009) was considered to represent a typical sedimentary system that might be affected by CO_2 and brine leakage from an underlying storage reservoir. As described in Figure 1c, the model dimension is 10000 m $\times$ 5000 m $\times$ 240 m in x, y, and z, directions. Three-dimensional heterogeneity with binary faces (sand and clay) is characterized and represented by faces-volume fraction and spatial correlation lengths of clay using well logs from the High Plains aquifer and T-PROGS code (Carle, 1999), which derives transition-probability based on conditional well logs.

Equilibrium chemistry with aqueous carbonate speciation and calcium carbonate dissolution and precipitation is assumed. Liquid-phase CO_2 concentration in groundwater will enhance calcite dissolution by the following reactions:

$$CO_2\ (g) \rightleftharpoons CO_2\ (aq) \tag{1}$$

$$CO_2\ (aq) + H_2O \rightleftharpoons HCO_3^- + H^+ \tag{2}$$

$$CaCO_3\ (calcite) + H^+ \rightleftharpoons Ca^{2+} + HCO_3^-. \tag{3}$$

These reactions will result in a change in solution pH. For the sake of methodology demonstration, the plume volume is defined for water with pH < 6.5 and is considered as one measure for risk assessment. Assuming brine is dominated by dissolved sodium and chloride, the aquifer volume for TDS > 1500 mg L^{-1} is calculated as a measure for assessing the effect of brine leakage on groundwater. Risk profiles could be derived for other pH and TDS thresholds.

2.4. Methodology of Uncertainty Quantification

As defined in Table 1, all inputs except x_{13} can freely vary over their entire ranges of uncertainty. The corresponding uncertainty of a model output, such as CO_2 and brine leakage rate, is measured by its variance (Saltelli et al., 2008).

In Figure 2, $x_i,\ i = 1, 2, \cdots, 13$, are dimensions of parametric space as defined in Table 1, **RS**, **FT**, and **AQ** stand for numerical models of reservoir, fault, and aquifer, respectively; x, y, and z, are Cartesian coordinates; P is pressure; and S_c and S_b are CO_2 and brine saturation; q_c and q_b are their fluxes at the fault outlet; and x_{13} is an intermediate variable defined as the logarithmic mean of sand and clay permeability

$$x_{13} = x_1 x_4 + (1 - x_1) x_5 \tag{4}$$

and used as a lumped aquifer permeability in the RS model with coarse aquifer grids. To address the effect of aquifer heterogeneity on geochemical processes, sand and clay permeabilities are distinguished in the AQ model with a higher mesh resolution.

The statistical approximation of risk-relevant measures in terms of all uncertain parameters is described as

$$y = a_0 + \overbrace{\sum_i a_i x_i}^{\text{1st-order}} + \overbrace{\sum_i \sum_j a_{ij} x_i x_j}^{\text{2nd-order}} + \overbrace{\sum_i \sum_j \sum_k a_{ijk} x_i x_j x_k}^{\text{3rd-order}} + \overbrace{\cdots}^{\text{high-order}} \tag{5}$$

where a_0, a_i, a_{ij}, a_{ijk}, and $a_{ijk...}$ are coefficients of polynomial fitting, and i, j, and k are input indices. The statistical approximation of y is also called an emulation, a response surface, a reduced-order model (ROM), a surrogate model (Sun et al., 2012a), a system-level model (Stauffer et al., 2009), a metamodel, proxy model, or a *model of models* (Razavi et al., 2012). Response surfaces are constructed for (1) pressure and CO_2 and brine saturation from RS model at a fault inlet with an unknown location, (2) CO_2 and brine fluxes from FT model at the fault outlet, and (3) aquifer volume affected by CO_2 and brine leakage.

The proposed global sampling method is implemented by the following steps:

1. Define parametric space $\mathcal{R}^m$ with parameter ranges and distributions, where m is the number of uncertain inputs.
2. Generate N global sample points that are uniformly and log-uniformly distributed in the m-dimensional space.
3. Assign sub-space of N sample points to physics-specific sub-models.
4. Run sub-models sequentially with propagation of system variables.
5. Construct response surfaces of system outputs in terms of direct and indirect uncertain inputs.
6. Conduct sensitivity analysis and generate overall risk profiles.

The quality of regression is evaluated by the model coefficient of determination (Saltelli et al., 2008)

$$R^2 = \frac{\sum_{i=1}^{N} (\hat{y}_i - \bar{y})^2}{\sum_{i=1}^{N} (y_i - \bar{y})^2} \tag{6}$$

where y_i and $\hat{y}_i$ are simulated and emulated model results, $\bar{y}$ is the mean of simulated results. $R^2 \in [0,\ 1]$ represents the fraction of the model output variance accounted for by the response surface.

The constructed response surfaces are computationally efficient for emulating a greater number of sampling points for sensitivity analysis, risk assessment, and decision optimization.

3. Results and Discussion

Emulation is designed for modeling multi-component reactive transport, which is characterized by the 12-dimensional uncertain parametric space (Table 1) and computationally demanding simulations. We employ Latin hypercube sampling (McKay et al. 1979; Iman et al. 1981) to generate 1000 sample points for building the NUFT models representing the RS, FT, and AQ subsystems. Third-order response surfaces are developed from the Latin hypercube samples for emulating (1) pressure and CO_2/brine saturation at the fault inlet, (2) CO_2 and brine fluxes at the fault outlet, and (3) aquifer volume affected by CO_2 and brine leakage.

3.1. Deterministic Simulation

Sample 418 is randomly selected from 1000 sample points to demonstrate the simulation processes and risk assessment. For the parameter values given in Table 2, the reservoir, fault-leakage, and aquifer models are deterministic and simulated sequentially using the

NUFT code (Nitao, 1998; Hao et al., 2012). The first three parameters (sand volume fraction, correlation lengths of clay in x and z directions) are used to determine heterogeneous structure of the shallow aquifer by using the T-PROGS code (Carle and Fogg, 1996, 1997; Carle, 1999). The AQ-model mesh file is generated according to the sand-clay structure (Figure 3). It is assumed that the existing fault at the distance x_{12} does not release reservoir pressure significantly. Therefore, pressure and saturation profiles along the fault are derived by post-processing RS outputs without considering the fault explicitly in the RS mesh file.

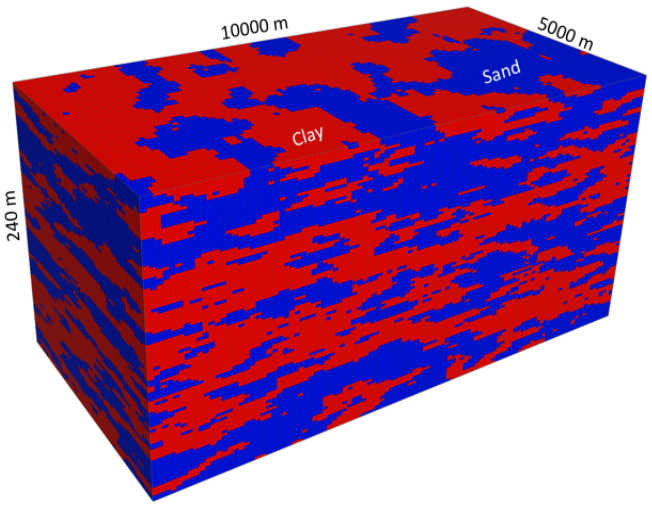

Figure 3. Heterogeneous aquifer model of sample 418 simulated using T-PROGS and well logs in High Plains Aquifer. Red and blue represent clay and sand, respectively. Note that vertical scale is exaggerated.

In the context of non-intrusive uncertainty quantification, a sample point, such as the 418th point, represents a coordinate (see Table 2) in the 12-dimensional parametric space. The NUFT model outputs of interest are plotted in Figure 4 as functions of time. Pressure (Figure 4a) and saturation (Figure 4b) profiles, generated by running the RS model for sample 418, are inputs to the FT model of sample 418. The FT model of sample 418 is then evaluated to produce CO_2 and brine fluxes (Figure 4c) at the fault outlet. These fluxes are in turn fed to AQ model for predicting concentration profiles and risk measures (Figure 4c).

Table 2. System parameters of sample 418.

Param.	Value	Param.	Value	Param.	Value
x_1	0.4875 [-]	x_5	1.0139×10^{-16} [m^2]	x_9	5.0431×10^{-14} [m^2]
x_2	881.4815 [m]	x_6	900.0000 [m]	x_{10}	9.7947×10^{-14} [m^2]
x_3	9.5250 [m]	x_7	1.7108 [mol kg^{-1}]	x_{11}	73.2232 [kg s^{-1}]
x_4	3.6187×10^{-11} [m^2]	x_8	4.2133×10^{-17} [m^2]	x_{12}	536.9369 [m]
$x_{13} = x_1x_4 + (1-x_1)x_5$					5.1652×10^{-14} [m^2]

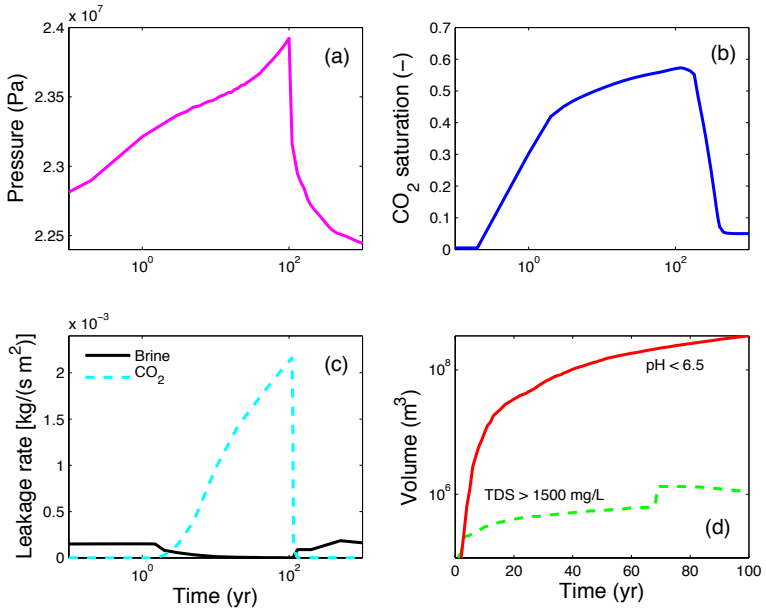

Figure 4. Deterministic outputs of sample 418. (a) Pressure at fault inlet. (b) CO_2 saturation at fault inlet. (c) CO_2 and brine fluxes at fault outlet. (d) Plume volume defined by pH < 6.5 and TDS > 1500 mg L^{-1}.

Among many other risk measures, we are interested in the total aquifer volume defined by EPA drinking water standards in pH and TDS. As seen in Figures 5 and 6, isosurfaces of pH $= 6.5$ and TDS $= 1500$ mg L^{-1} are derived from AQ concentration profiles, and the volume within those isosurfaces is integrated spatially as a function of time

$$U_p = \int_\Omega u(x,y,z)du\Big|_{\text{pH}<6.5}, \quad U_t = \int_\Omega u(x,y,z)du\Big|_{\text{TDS}>1500} \tag{7}$$

where U_p and U_t are aquifer volume defined by pH < 6.5 and TDS > 1500 mg L^{-1}, respectively; Ω denotes the spatial domain; and u is the elementary volume at x, y, z. As shown in Figure 4d, the total aquifer volume impacted by CO_2 and brine leakage for pH and TDS, respectively, becomes a risk measure as a function of time.

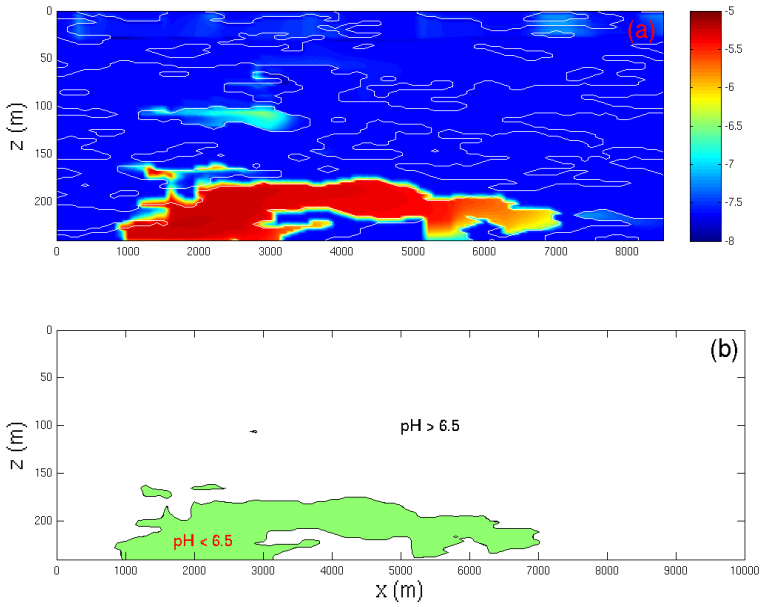

Figure 5. pH-defined aquifer plume on $x \sim z$ plane for $y = 0.0$ m and $t = 100$ years. (a) Contour of $log_{10}H^+$. White line indicates the divide between sand and clay. (b) Contaminated aquifer volume defined by pH < 6.5.

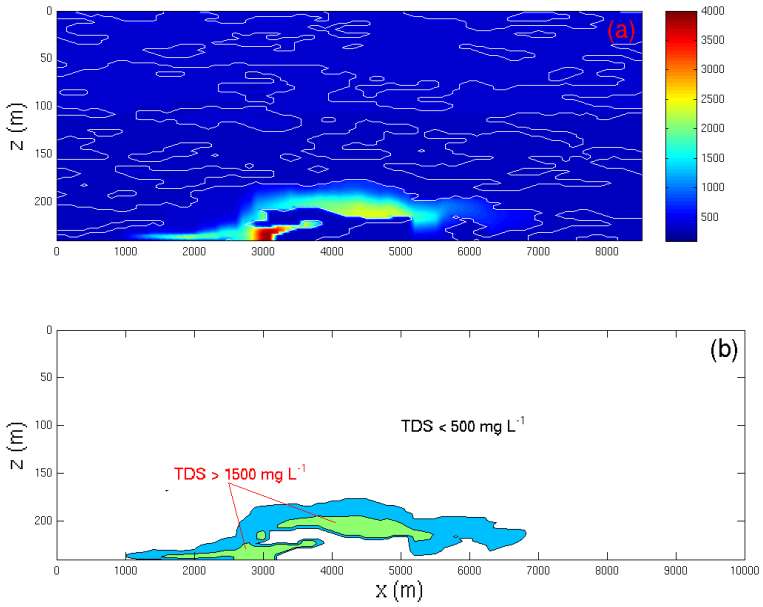

Figure 6. TDS-defined aquifer plume on $x \sim z$ plane for $y = 0.0$ m and $t = 100$ years. (a) TDS distribution. (b) Contaminated aquifer volume defined by TDS > 500 (blue and green) and by TDS > 1500 (green) mg L^{-1}.

To conduct uncertainty quantification and risk assessment, we repeated the same simulation process for 1000 sample points in the 12-dimensional space. In Sec. 3.2 $\sim$ Sec. 3.4, the PSUADE code (Tong, 2005, 2010) is used for constructing response surfaces of risk-relevant

measures and intermediate variables. We give details for using the PSUADE uncertainty quantification library (Tong, 2005) to construct response surfaces of risk-relevant measures and intermediate variables.

3.2. Reservoir Model Results

One of the risk measures for CO_2 storage is pressure buildup, which could elevate the probability of re-activating faults and cause CO_2 and brine leakage to groundwater aquifers or the atmosphere. Scatter plots of the peak pressure at the fault inlet (Ⓐ in Figure 1a), from 1000 simulations, are given in Figure 7 in terms of permeabilities of groundwater aquifer, storage reservoir, and caprock (x_{13}, x_{10}, x_8), CO_2 injection rate (x_{11}), and the distance between the injector and fault (x_{12}). We observe a clear dependence of the peak pressure on caprock permeability and a slight dependence on reservoir permeability and injection rate. Quantitatively, we compute the Sobol' sensitivity indices for x_8, x_{10}, x_{11}, x_{12}, x_{13} to be [0.8390 0.0853 0.1041 0.0025 0.0000], respectively. Taking the peak pressure as an example, the response surface is constructed using third-order polynomial regression (Eq. 5) and verified by comparing system-level emulations with process-level simulations on prescribed sample points in Figure 8.

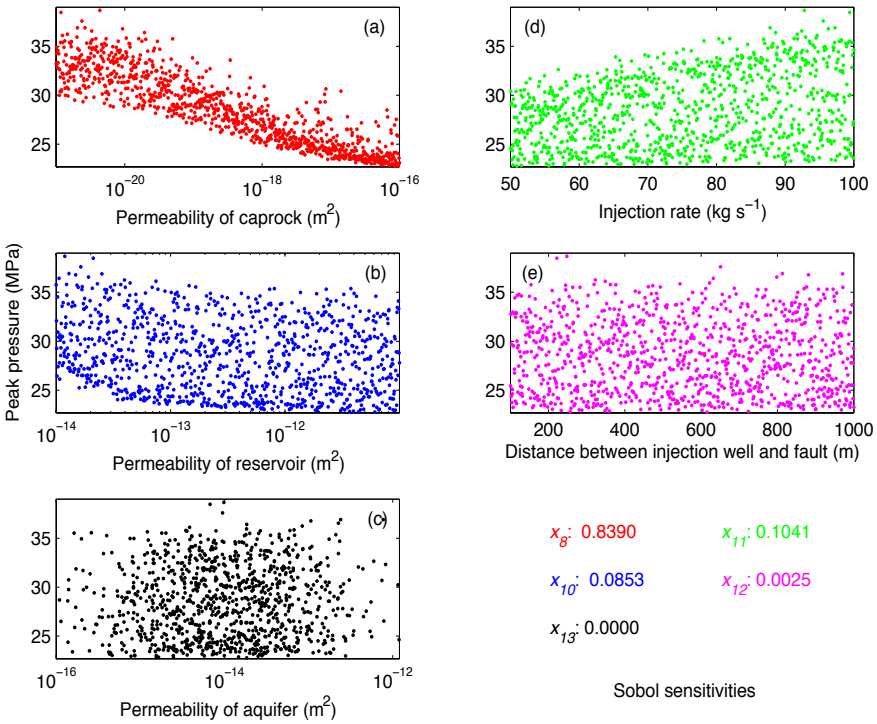

Figure 7. Scatter plots of peak pressure at fault inlet as a function of uncertain parameters. Subplots (a), (b), and (c) show a strong, slight, and zero dependence of peak pressure on caprock permeability (x_8), reservoir permeability (x_{10}), and lumped aquifer permeability (x_{13}), respectively. Subplot (d) shows a slight and positive dependence of the peak pressure on injection rate (x_{11}). Subplot (e) show little sensitivity of the distance between the injector and the fault (x_{12}).

We conducted Sobol' sensitivity analysis of pressure and CO_2 saturation from RS model, as well as CO_2 and brine fluxes from FT model and aquifer volume contaminated by CO_2 and brine leakage from AQ model, the result of which is shown in Table 3. We qualitatively

categorize parameter sensitivities into four groups (1) very important (>0.75), (2) important (0.5∼0.75), (3) insignificant (0.2∼0.5), and (4) irrelevant (<0.2). Reservoir permeability is the most sensitive parameter to the pressure profile at the fault inlet in the early time (< 20 yr), but quickly reduces its role as time progresses. By contrast, caprock permeability is an insensitive parameter initially to the pressure profile, but becomes the dominant parameter in later time (> 80 yr). In the ealy stage of injection, the radial and horizontal advection from the injector, as the main transport process to spread CO_2 plume, depends on the reservoir permeability. This explains the higher sensitivity of reservoir permeability in the early stage. As CO_2 plume spreads to a certain size, the radial expansion of CO_2 plume becomes slower with a constant injection rate. Then, the tightness of caprock becomes a sensitive parameter. For CO_2 saturation, reservoir permeability is the sole sensitive parameter. Since the shallow aquifer is far (2000 m) from the storage reservoir, the lumped aquifer permeability (x_{13}) does not show any contribution to pressure and saturation profiles.

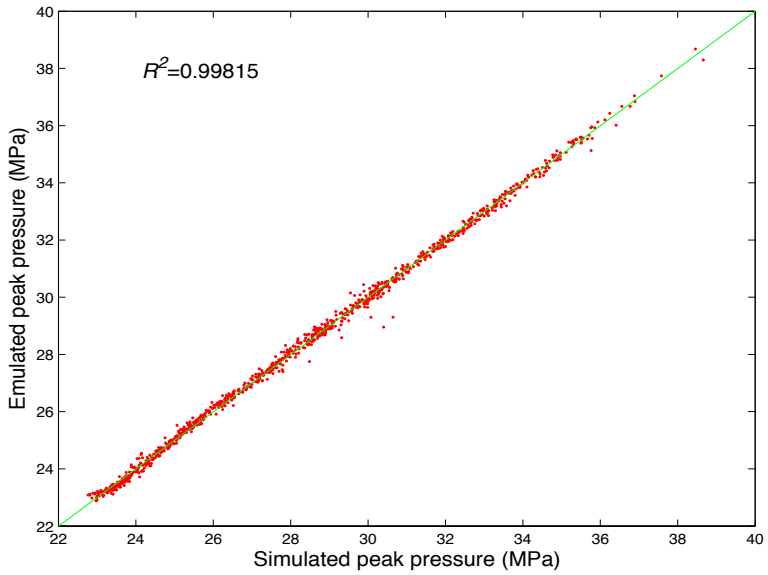

Figure 8. Comparison of simulated and emulated peak pressure at fault inlet (see Figure 1a).

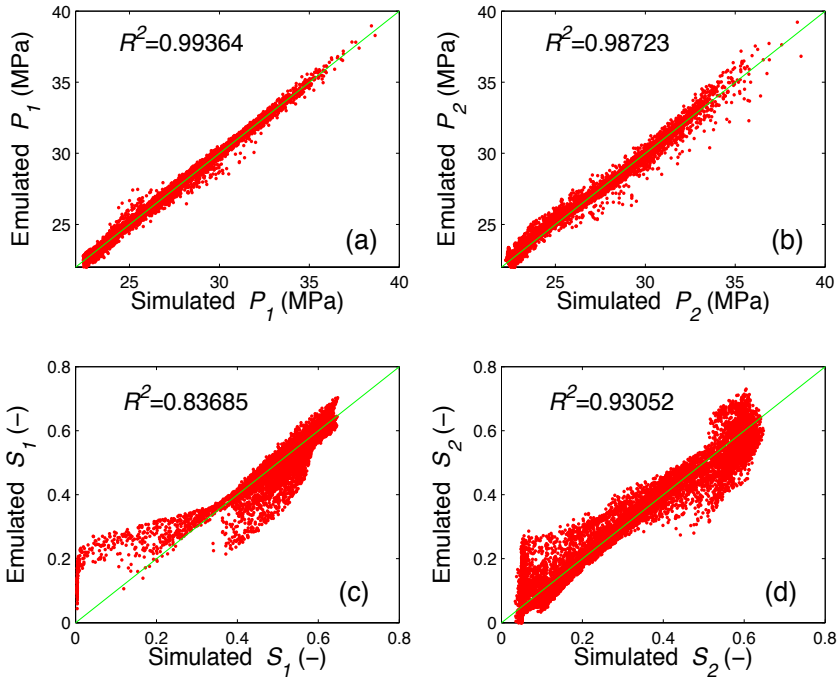

Figure 9. Comparison of simulated and emulated pressure and CO_2 saturation at fault inlet using time-included ROMs. (a) Simulation-emulation (S-E) comparison of pressure in injection period. (b) S-E comparison of pressure in post-injection period. (c) S-E comparison of CO_2 saturation in injection period. (d) S-E comparison of CO_2 saturation in post-injection period.

Since RS-model outputs, such as pressure and CO_2/brine saturation at fault inlet, are time dependent, we expect to treat time as a special dimension in ROM construction. As such, a single ROM will represent the dynamic process over the entire simulation period. Otherwise, multiple ROMs should be constructed separately in each time interval. If an output is a monotonic function of time, the time dimension can be added for constructing the ROM by using polynomial fitting. Although both pressure and saturation curves are not monotonic over 1000-year simulation time, they are monotonic in injection ($t < 100$ yr) and post-injection ($t \geq 100$ yr) periods. Therefore, two separate ROMs are developed, respectively for pressure and CO_2 saturation, in those two periods with considering time dimension. Comparisons between the simulated and emulated (ROMs) results are plotted in Figure 9.

The advantage of a single ROM with time dimension over multiple ROMs in time is ease of data processing and transferring. However, there are limits of the total number of sample points for various response surface methods and a given computer memory. It is also worth comparing the emulation quality of time-included ROM and time-excluded ROMs. As shown in Figure 10, the stepwise (or time specific) ROMs agree better with simulations than time-included ROM (Figure 9). Figure 11 indicates that the dynamic R^2 indices of stepwise ROMs for both pressure and saturation profiles are preferred.

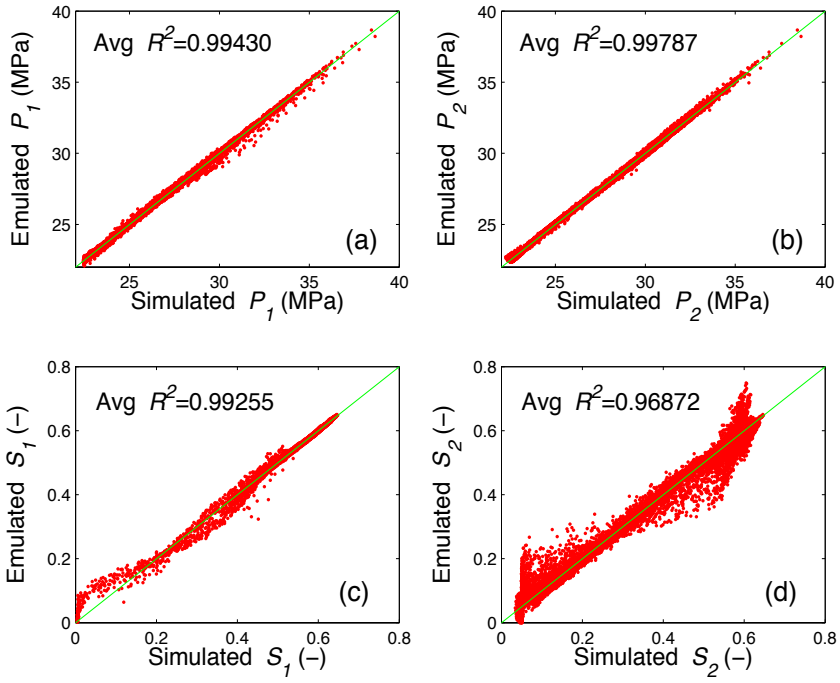

Figure 10. Comparison of simulated and emulated pressure and CO_2 saturation at fault inlet using stepwise ROMs. (a) S-E comparison of pressure in injection period. (b) S-E comparison of pressure in post-injection period. (c) S-E comparison of CO_2 saturation in injection period. (d) S-E comparison of CO_2 saturation in post-injection period.

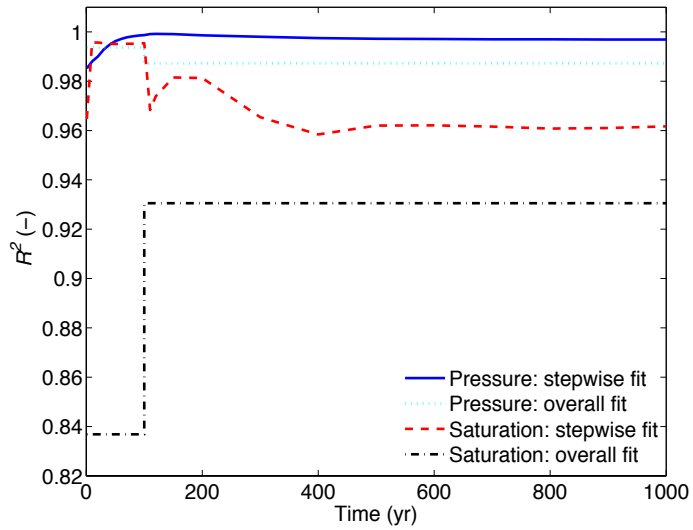

Figure 11. Comparison of R^2 indices. The R^2 indices of overall fitting for both pressure and saturation profiles are lower than those of stepwise fitting.

Although we have used uniform and log-uniform distributions of uncertain parameters listed in Table 1 to construct response surfaces of pressure and CO_2/brine saturation at the fault inlet, uncertainty of those outputs is reduced by using normal or log-normal distribu-

tions for some uncertain parameters. If caprock and reservoir permeabilities take log-normal didstriutions, such as $\log_{10}x_8 = \mathcal{N}(-18.5, 0.5)$ and $\log_{10}x_{10} = \mathcal{N}(-12.5, 0.3)$, and injection rate x_{11} and distance between fault and injector x_{12} keep their uniform distributions, pressure and saturation at the fault inlet at 100,000 Monte Carlo sample points are emulated on previously constructed response surfaces. Figures 12 and 13 show the pressure and saturation profiles with confidence levels.

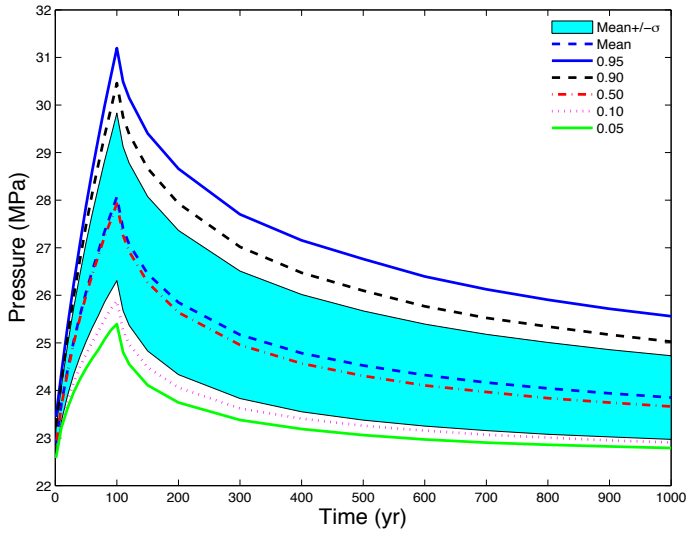

Figure 12. Pressure at fault inlet as a function of time for various confidence levels. The shaded area covers one standard deviation above and below mean value.

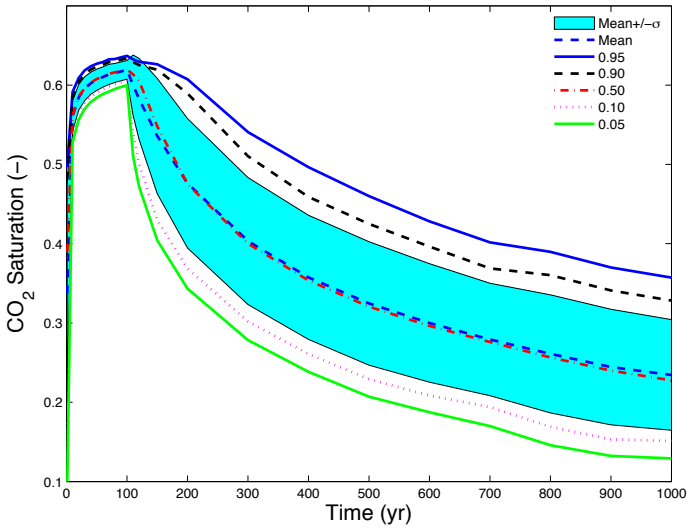

Figure 13. CO_2 saturation at fault inlet as a function of time for various confidence levels. The shaded area covers one standard deviation above and below mean value.

Uncertainties of pressure and CO_2 saturation at the fault inlet can be visualized using probability density functions (PDFs) for given times. As shown in Figure 14, PDFs of pressure and saturation with log-normal distribution of reservoir and caprock permeabilities

(Figures 14a, c) display normal or near normal distributions at specified times. PDFs of pressure and saturation with log-uniformly distributed permeabilities (Figures 14b, d) display left-skewed and flat-bimodal distributions, respectively.

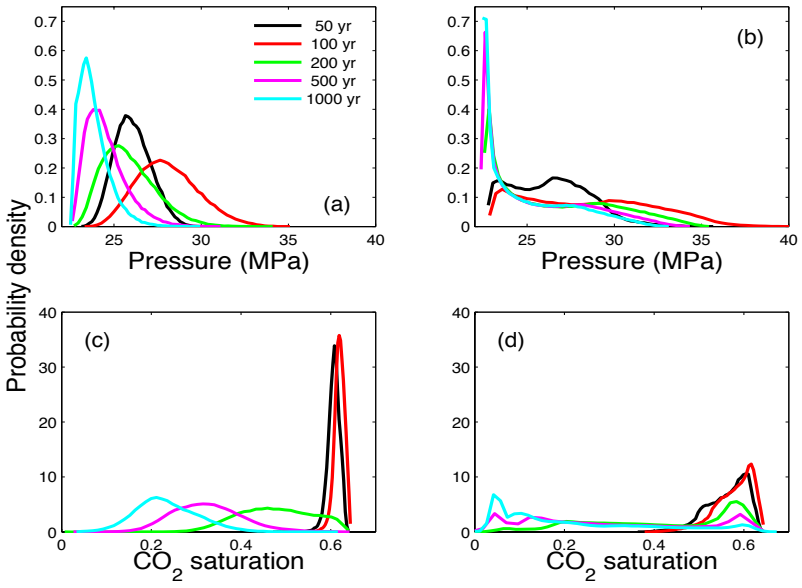

Figure 14. Time evolution of probability density distribution of pressure and CO_2 saturation at fault inlet. (a) Pressure PDF with *log-normal* distribution of x_8 and x_{10}. (b) Pressure PDF with *log-uniform* distribution of x_8 and x_{10}. (c) Saturation PDF with *log-normal* distribution of x_8 and x_{10}. (d) Saturation PDF with *log-uniform* distribution of x_8 and x_{10}.

3.3. Fault-leakage Model Results

Similar to pressure and saturation profiles from the reservoir model, CO_2 and brine fluxes at fault outlet (Ⓑ in Figure 1b) behave non-monotonically with time. To facilitate the construction of reduced-order models, we take cumulative fluxes, which are monotonic with time, as the model output. Six uncertain parameters, (caprock, fault, and reservoir permeabilities, x_8, x_9, x_{10}, injection rate x_{11}, distance between fault and injector x_{12}, and lumped aquifer permeability x_{13}), contribute to CO_2 and brine fluxes directly and indirectly at the fault output. As seen in Table 3 and Figure 15, Sobol' sensitivity analysis indicates that fault permeability most impacts the uncertainty of CO_2 flux, while both fault permeability and caprock permeability are equally important to brine flux. Detailed description and analysis of CO_2 phase transition and physical properties along the fault can be found in Lu et al. (2012).

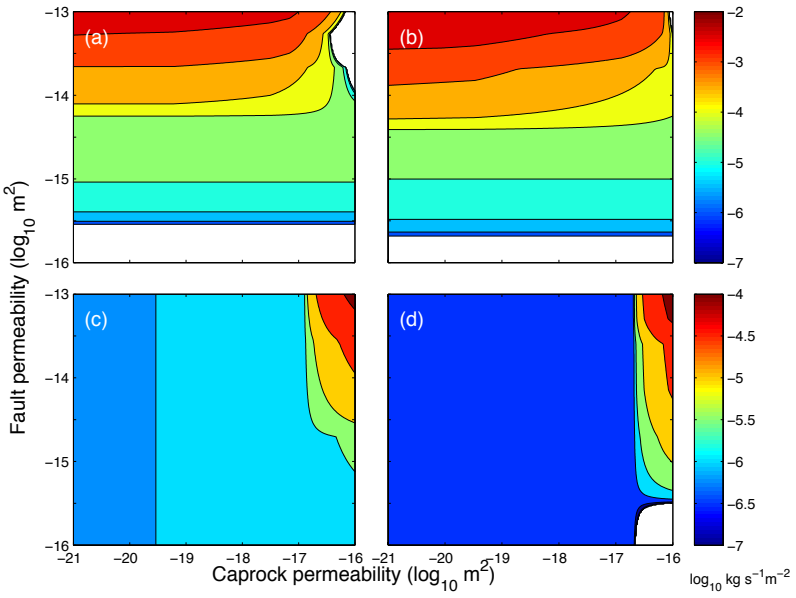

Figure 15. Snapshots of CO_2/brine fluxes at fault outlet as functions of caprock and fault permeabilities. (a)(b) CO_2 flux at 50 and 100 years. (c)(d) Brine flux at 50 and 100 years. White area indicates zero flux.

Figures 16 and 17 show the cumulative fluxes of CO_2 and brine at the fault outlet at various confidence levels, emulating 100,000 Monte Carlo sample points on the response surfaces. We observe that CO_2 and brine flux curves are not as smooth as those of pressure and saturation profiles in Figures 12 and 13. This may be due to uncertainties of fault and caprock permeabilities. Figure 18 shows probability density distributions of cumulative CO_2 and brine fluxes at different times.

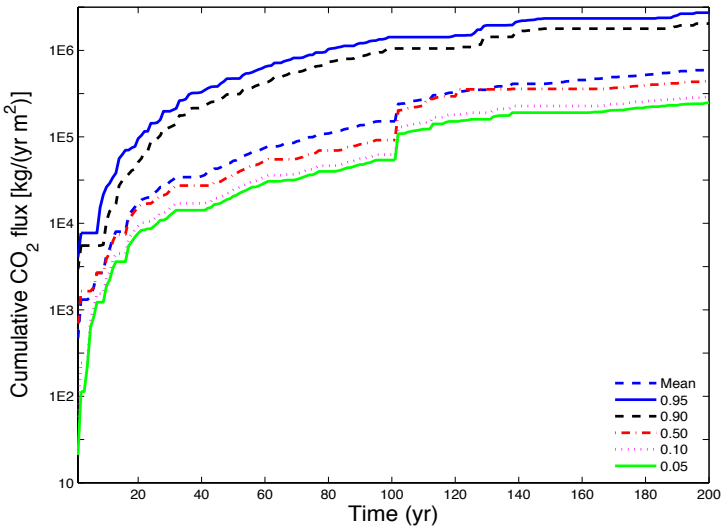

Figure 16. Cumulative CO_2 flux as a function of time at various confidence levels.

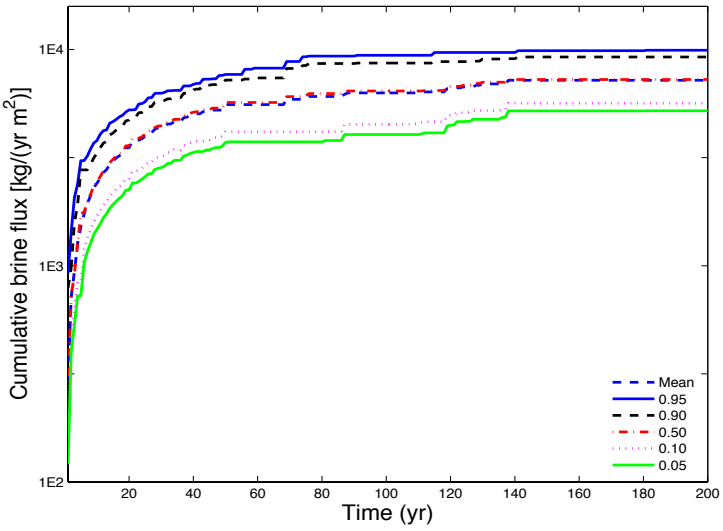

Figure 17. Cumulative brine flux as a function of time at various confidence levels.

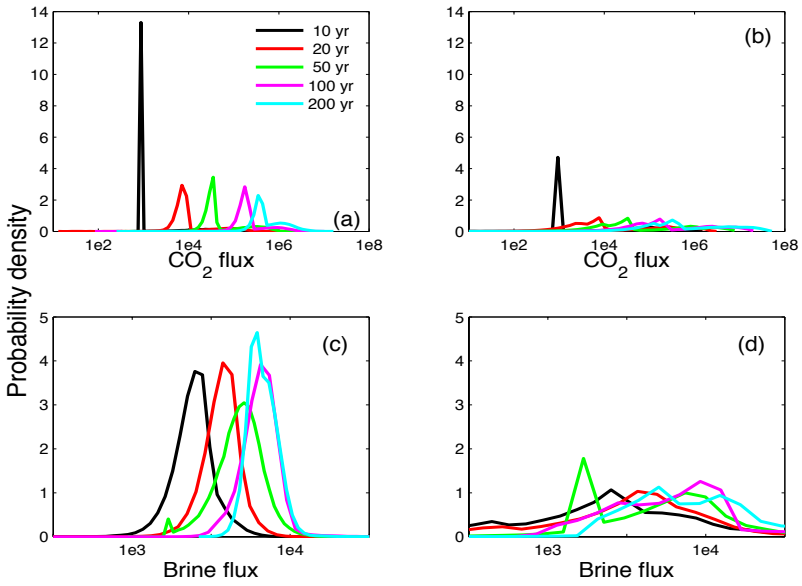

Figure 18. Time evolution of probability density distributions of cumulative CO_2 and brine fluxes (kg $yr^{-1}m^{-2}$) at fault outlet. (a) PDF of CO_2 flux with *log-normal* distribution of x_8, x_9, and x_{10}. (b) PDF of CO_2 flux with *log-uniform* distribution of x_8, x_9, and x_{10}. (c) PDF of brine flux with *log-normal* distribution of x_8, x_9, and x_{10}. (d) PDF of brine flux with *log-uniform* distribution of x_8, x_9, and x_{10}.

3.4. Aquifer Model Results

To assess the risk of CO_2 leakage to an aquifer, we first define plume volume as a measure bounded by EPA MCL standards pH < 6.5 and TDS > 1500 mg L^{-1} (Eq. 7). Sobol' sensitivity indices show that the total sensitivity of an uncertain parameter may vary over time. Taking the pH-defined plume volume as a measure, uncertain parameters are cate-

gorized into 4 groups, as shown in Figure 19: (1) parameters x_i, $i = 2, 3, 4, 5, 7, 11,$ and 12 show their early-time importance, but diminish as time progresses; (2) parameters x_i, $i = 1, 8, 10$ maintain a small, but constant role over time; (3) parameter x_6 plays a constant and moderate role; and (4) parameter x_9 keeps its increasing and dominating contribution to the uncertainty of pH-defined volume. Although fault permeability (x_9) is not a direct input to AQ process model, its uncertainty dominates the uncertainty of AQ model output through the source-term of CO_2 and brine fluxes.

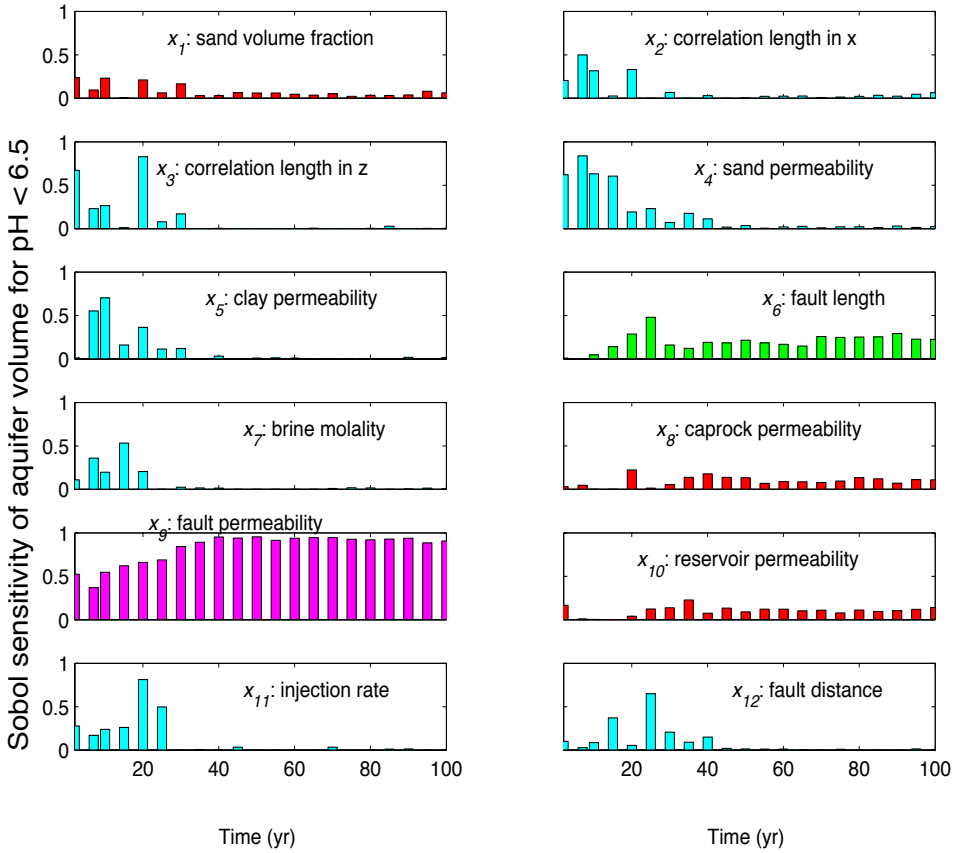

Figure 19. Sobol' total sensitivity of aquifer volume for pH < 6.5. Red group (x_1, x_8, x_{10}): constant but minor contribution. Cyan group (x_i, $i = 2, 3, 4, 5, 7, 11,$ and 12): early-time contribution. Green group (x_6): constant and moderate contribution. Magenta group (x_9): increasing and dominating contribution.

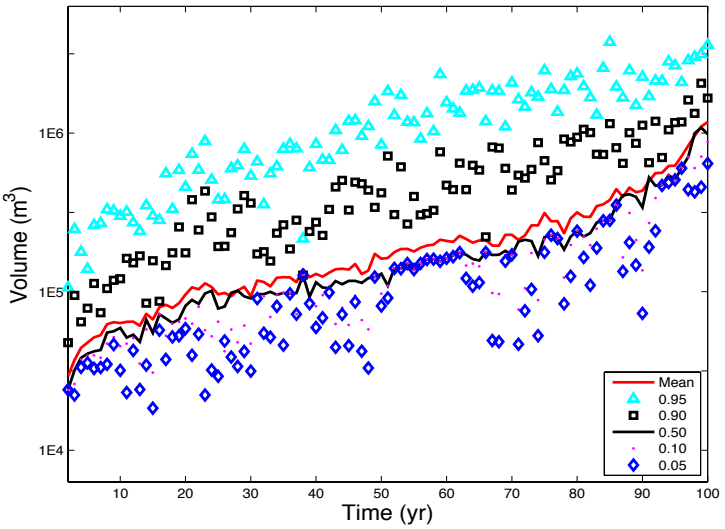

339 **Figure 20.** Aquifer volume contaminated by CO_2 leakage (pH $<$ 6.5).

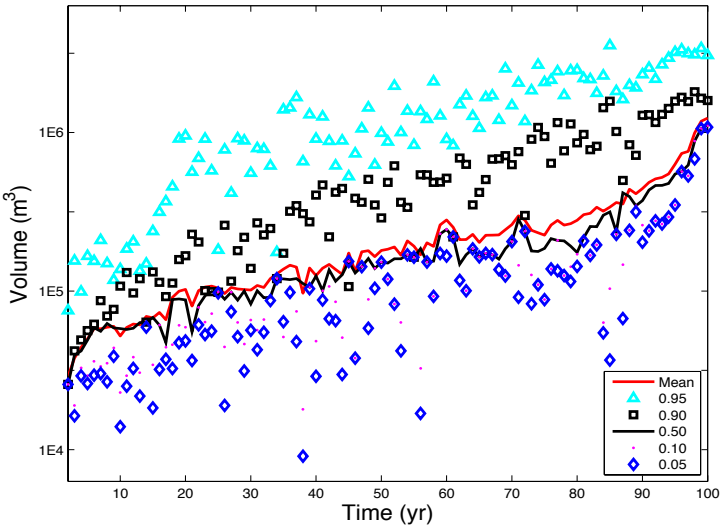

340 **Figure 21.** Aquifer volume contaminated by CO_2 leakage (TDS $>$ 1500 mg L^{-1}).

341 To better understand the uncertainty of aquifer volume contaminated by CO_2 and brine
342 leakage, we examine the time evolution of probability densities (PDFs). PDFs are computed
343 with the response surfaces of contaminated aquifer volume by Monte Carlo sampling using
344 lognormal and log-uniform distributions on the uncertain inputs 4, 5, 8, 9, and 10 (see Table
345 1). The PDFs of the volume defined by pH $<$ 6.5 and TDS $>$ 1500 mg L^{-1} are observed to
346 shift toward high values and exhibit wider standard deviation as time progresses (Figures
347 20 and 21). We observe that the skewnesses of the volume distribution at most time steps
348 are positive and monotonically increase with time, reflecting a longer tail on the right side
349 of the mean value on the logarithm scale. The high values of kurtosis (100$\sim$7000) at all time
350 steps indicate the "peak-like" distributions as shown in Figure 22.

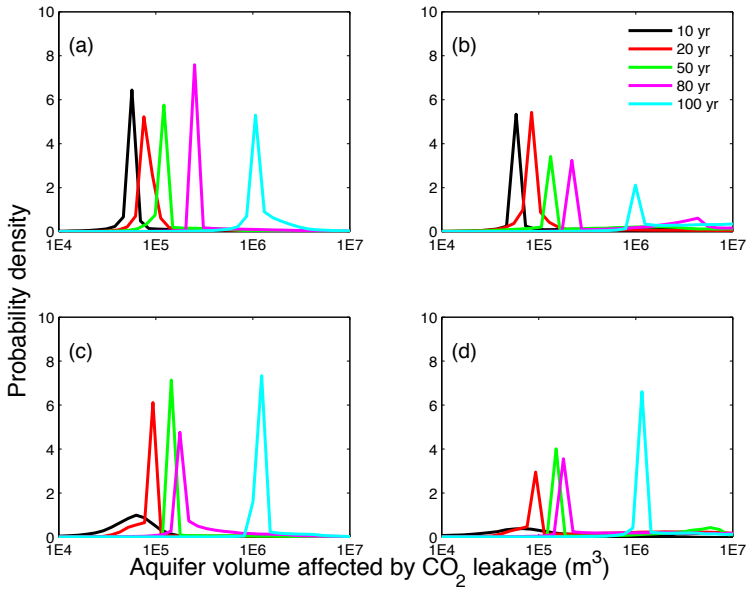

Figure 22. Time evolution of probability density distribution of aquifer volume contaminated by CO_2 leakage. (a) Aquifer volume defined by pH < 6.5 and with normal distributions of x_i, $i = 4, 5, 8, 9, 10$. (b) Aquifer volume defined by pH < 6.5 and with uniform distributions of those inputs. (c) Aquifer volume defined by TDS > 1500 mg L^{-1} and with normal distributions of those inputs. (d) Aquifer volume defined by TDS > 1500 mg L^{-1} and with uniform distributions of those inputs.

4. Conclusions

In this paper, we proposed a global sampling method and developed an integrated simulation-emulation system to study uncertainty propagation through physics-specific subsystems and assess leakage-relevant risk profiles for CO_2 geological sequestration. For demonstrative purposes, we considered hypothetical reservoir and fault subsystems and a realistic aquifer with multiple geological realizations, which are conditional to wellbore logs in High Plains aquifer. Parameter uncertainties and uncertainty due to aquifer heterogeneity are parameterized in three physics-specific simulations. Pressure buildup in storage reservoir, CO_2 and brine leakage rates through fault, and aquifer volume contaminated by CO_2 and brine leakage are considered as risk measures. Uncertainties of these risk measures are quantified as functions of uncertain parameters. Key findings in this paper are summarized as the following:

1. Uncertainty quantification and risk assessment of CO_2 geologic sequestration can be conducted on reduced-order models, which are developed from computationally expensive simulations in the space of uncertain parameters.

2. Pressure buildup in reservoir storage is sensitive to reservoir and caprock permeabilities. CO_2 saturation mainly depends on reservoir permeability.

3. Due to CO_2 phase change and buoyant flow, CO_2 leakage rate though fault mainly depends on fault permeability. In contrast with CO_2 leakage rate, other uncertain parameters, such as reservoir, caprock, and aquifer permeabilities, injection rate, and the distance between fault and injector, all contribute to brine leakage rate.

4. Contaminated aquifer volume is evaluated from AQ model outputs by using EPA drinking water standards pH=6.5 and TDS = 1500 mg L^{-3}. The uncertainty of pH-defined volume mainly results from the uncertainty of fault permeability. Although the fault permeability is an indirect input to AQ model, its uncertainty is propagated to AQ model through FT model output, CO_2 leakage rate.

5. Material volume fraction and spatial correlation lengths, which determine the heterogeneity of the High Plains aquifer, control the plume shape of pH- and TDS-defined aquifer volume. A small vertical correlation length and a long horizontal correlation length prevent CO_2 release to atmosphere.

6. Compared to local-system sampling, relationship between risk measures and indirect inputs can be developed by using the global sampling. Otherwise, it is difficult, at least tedious, to parameterize the time-dependent CO_2 and brine leakage rates as uncertain inputs to AQ models.

7. In the parametric space of FT models, there is a hyper-dimensional and time-dependent isosurface, which divides leaky and safe domains. Within the leakage domain, CO_2 and leakage rates are provided with probability distribution.

8. Time can be considered as a special dimension in parametric space to use PSUADE for constructing response surfaces (ROMs) of system outputs, which are monotonic functions of time. However, stepwise ROMs without considering time dimension better represent physical systems than the overall, but single, ROM including time dimension.

Assessment of prediction uncertainty and uncertainty propagation due to uncertain model inputs and geologic structure is a part of risk assessment for CO_2 geologic sequestration. We have demonstrated the application of PSUADE code for sampling, response-surface construction, and sensitivity analysis. By using T-PROGS code, we described the qualitative geologic structure by using quantitative uncertain parameters (material volume fraction, spatial correlation lengths) and further studied the impact of aquifer heterogeneity on CO_2/brine leakage-relevant risk profiles.

This work is limited to non-intrusive (sampling-based) schemes. For the simplicity in coupling with deterministic simulation codes in different modules, sampling-based schemes require a minimal coding effort. However, each simulation code is treated as a block box and uncertainty propagation is only measured through input-output statistics. To track uncertainty propagation through governing equations within a code, intrusive UQ methods are necessary (Chen et al., 2012).

Acknowledgements

The authors wish to thank David Ortiz-Suslow at the University of Miami and Thomas Wolery at Lawrence Livermore National Laboratory for their careful review and helpful comments that led to an improved manuscript. This work was supported in part by the National Risk Assessment Partnership (NRAP) and the Carbon Capture Simulation Initiative (CCSI) through the National Energy Technology Laboratory, and performed under the auspices of the U.S. Department of Energy by Lawrence Livermore National Laboratory under contract DE-AC52-07NA27344.

References

Apps, J.A., Zheng, L., Zhang, Y., Xu, T., Birkholzer J.T., 2010. Evaluation of potential changes in groundwater quality in response to CO_2 leakage from deep geologic storage, *Transp. Porous Med.* **82**(1), 215–246.

Bachu, S., 2008. CO_2 storage in geological media: Role, means, status, and barriers to deployment, *Prog. Energ. Combust.* **34**(2), 254–273.

Birkholzer, J.T., Zhou, Q., Tsang, C.-F., 2009. Large-scale impact of CO_2 storage in deep saline aquifers: a sensitivity study on the pressure response in stratified systems, *Int. J. Greenh. Gas Control* **3**(2), 181–194.

Buscheck, T.A., Sun, Y., Hao, Y., Wolery, T.J., Bourcier, W., Tompson, A.F.B., Jones, E.D., Friedmann, S.J., Aines, R.D., 2011. Combining brine extraction, desalination, and residual-brine reinjection with CO_2 storage in saline formations: Implications for pressure management, capacity, and risk mitigation, *Energy Procedia* **4**, 4283–4290.

Buscheck, T.A., Sun, Y., Chen, M., Hao, Y., Wolery, T.J., Bourcier, W.L., Court, B., Celia, M.A., Friedmann, S.J., Aines, R.D., 2012. Active CO_2 reservoir management for carbon storage: Analysis of operational strategies to relieve pressure buildup and improve injectivity, *Int. J. Greenh. Gas Control* **6**, 230–245.

Carle, S.F., Fogg, G.E., 1996. Transition probability-based indicator geostatistics, *Math. Geol.* **28**(4), 453–476.

Carle, S.F., Fogg, G.E, 1997. Modeling spatial variability with one- and multi-dimensional continuous Markov chains, *Math. Geol.* **29**(7), 891–918.

Carle, S.F., 1999. T-PROGS: Transitional probability geostatistical software users' guide, University of California, Davis.

Carroll, S., Hao, Y., Aines, R., 2009. Geochemical detection of carbon dioxide in dilute aquifers, *Geochem. T.* **10**(4), doi:10.1186/1467-4866-10-4, 1–18.

Chen, X., Ng, B., Sun, Y., Tong, C., 2012. A flexible uncertainty quantification method based on multi-physics decomposition: applications in reactive transport, *J. Comput. Phys.* Submitted.

Clement, T.P., Sun, Y., Hooker, B.S., Petersen, J.N., 1998. Modeling multi-species reactive transport in groundwater aquifers, *Ground Water Monit. Remediat.* **18**(2), 79–92.

Clement, T.P., Johnson, C.D., Sun, Y., Klecka, G.M., Bartlett, C., 2000. Simulation of natural attenuation at a chlorinated solvent contaminated site, *J. Contam. Hydrol.* **42**(2-4), 113–140.

Dai, Z., Wolfsberg, A., Lu, Z., Ritzi, R. Jr., 2007. Reprensenting aquifer architecture in macrodispersivity models with an analytical solution of the transition probability matrix, *Geophy. Res. Lett.* **34**(10), L20406.

Gasda, S.E., Bachu, S., Celia M.A., 2004. The potential for CO_2 leakage from storage sites in geological media: Analysis of well distribution in mature sedimentary basins, *Environ. Geol.* **46**(6-7), 707–720.

Celia, M.A., Nordbotten, J.M., Bachu, S., Dobossy, M., Court, B., 2008. Risk of leakage versus depth of injection in geological storage. In: Proceedings, 9th International Conference on Greenhouse Gas Control Technologies, Washington, D.C.

Guthrie, G.D., 2009. Bridging the basic-applied gap to provide the science base that ensures successful CO_2 sequestration, American Geophysical Union, Fall Meeting 2009, abstract H12B-02.

Hao, Y., Sun, Y., Nitao, J.J., 2012. Overview of NUFT – a versatile numerical model for simulating flow and reactive transport in porous media, Edited by Zhang et al. in *Ground water reactive transport model*, Bentham Science Publishers.

Iman, R.L., Helton, J.C., Campbell, J.E., 1981. An approach to sensitivity analysis of computer models, Part 1. Introduction, input variable selection and preliminary variable assessment, *J. Quality Technol.* **13**(3), 174–183.

Jordan, P.D., Oldenburg, C.M., Nicot, J.-P., 2011. Estimating the probability of CO_2 plumes encountering faults, *Greenh. Gas. Sci. Tech.* **1**(2), 160–171.

Keating, G.N., Middleton, R.S., Viswanathan, H.S., Stauffer, P.H., Pawar, R.J., 2011. How storage uncertainty will drive CCS infrastructure, *Energy Procedia* **4**, 2393–2400.

Liu, B., Zhang, Y., 2011. CO_2 modeling in a deep saline aquifer: a predictive uncertainty analysis using design of experiment, *Environ. Sci. Technol.* **45**(8), doi:10.1021/es103187b, 3504–3510.

Lu, C., Sun, Y., Buscheck, T.A., Hao, Y., White, J., Chiaramonte, L., Carroll, S.A., 2012. Uncertainty quantification of CO_2 leakage through a fault with multiphase and non-isothermal effects, submitted to *Greenh. Gas. Sci. Tech.*

McKay, M.D., Beckman, R.J., Conover, W.J., 1979. A comparison of three methods for selecting values of input variables in the analysis of output from a computer code, *Technometrics* **21**(2), 239–245, doi:10.2307/1268522.

Nitao, J.J., 1998. User's manual for the USNT module of the NUFT code, version 2 (NP-phase, NC-component, thermal), Lawrence Livermore National Laboratory, UCRL-MA-130653.

Pan, L., Oldenburg, C.M., Pruess, K., Wu, Y., 2011. Transient CO_2 leakage and injection in wellbore-reservoir systems for geologic carbon sequestration, *Greenh. Gas. Sci. Tech.* **1**(4), 335–350.

Pruess, K., 2011. Integrated modeling of CO_2 storage and leakage scenarios including transitions between super- and subcritical conditions, and phase change between liquid and gaseous CO_2, *Greenh. Gas. Sci. Tech.* **1**, 237–247.

Razavi, S., Tolson, T.A., Burn D.H., 2012. Review of surrogate modeling in water resources, *Water Resour. Res.* **48**, W07401, doi:10.1029/2011WR011527.

Refsgaard, J.C., Christensen, S., Sonnenborg, T.O., Seifert, D., Højberg, A.L., Troldborg, L., 2011. Review of strategies for handling geological uncertainty in groundwater flow and transport modeling, *Adv. Water Res.* **36**(1-2), 36–50.

Remoroza, A.I., Moghtaderi, B., Doroodchi, E., 2011. Coupled wellbore and 3D reservoir simulation of a CO_2 EGS, PROCEEDINGS, Thirty-Sixth Workshop on Geothermal Reservoir Engineering Stanford University, Stanford, California, January 31 - February 2, SGP-TR-191.

Saltelli, A., Ratto, M., Andres, T., Campolongo, F., Cariboni, J., Gatelli, D., Saisana, M., Tarantola, S., 2008. *Global Sensitivity Analysis. The Primer*, John Wiley & Sons.

Siirila, E.R., Navarre-Sitchler, A.K., Maxwell, R.M., McCray, J.E., 2012. A quantitative methodology to assess the risks to human health from CO_2 leakage into groundwater, *Adv. Water Res.* **36**(1-2), 146–164.

Sobol', I., 1993. Sensitivity estimates for nonlinear mathematical models, in Russian, *Matematicheskoe Modelirovanie* **2**, 112–118.

Sobol', I., 1990. Sensitivity analysis for nonlinear mathematical models, *Mathematical Modeling & Computational Experiment* **1**, 407–414, (English translation from Russian original paper Sobol', 1990).

Span, R., Wagner, W., 1996. A new equation of state for carbon dioxide covering the fluid region from the triple-point temperature to 1100K at pressures up to 800 MPa, *J. Phys. Chem. Ref. Data* **25**(6), 1509–1596.

Sun, Y., Buscheck, T.A., Lee, K.H., Hao, Y., James, S.C., 2010. Modeling thermal-hydrologic processes for a heated fractured rock system: impact of a capillary-pressure maximum, *Transp. Porous Med.* **83**(3), 501–523.

Sun, Y., Tong, C., Duan, Q., Buscheck, T.A., Blink, J.A., 2012a. Combining simulation and emulation for calibrating sequentially reactive transport systems, *Transp. Porous Med.* **92**(2), 509–526.

Sun, Y., Buscheck, T.A., Hao, Y., 2012b. An analytical method for modeling first-order decay networks, *Comput. Geosci.* **39**, 86–97.

Stauffer, P.H., Viswanathan, H.S., Pawar, R.J., Guthrie, G.D., 2009. A system model for geologic sequestration of carbon dioxide, *Environ. Sci. Technol.* **43**(3), 565–570.

Tartakovsky, D.M., Nowak, W., Bolster, D., 2011. Introduction to the special issue on

uncertainty quantification and risk assessment, *Adv. Water Res.* **36**(1-2), 1–2.

Tong, C., 2005. *PSUADE User's Manual*, Lawrence Livermore National Laboratory, LLNL-SM-407882.

Tong, C., 2010. Self-validated variance-based methods for sensitivity analysis of model outputs, *Reliab. Eng. Syst. Safe.*, **95**(3), 301–309.

Viswanathan, H.S., Pawar, R.J., Stauffer, P.H., Kaszuba, J.P., Carey, J.W., Olsen, S.C., Keating, G.N., Kavetski, D., Guthrie, G.D., 2008. Development of a hybrid process and system model for the assessment of wellbore leakage at a geologic CO_2 sequestration site, *Environ. Sci. Technol.* **42**(19), 7280–7286.

Yang, Y., Small, M.J., Ogretim, E.O., Gray, D.D., Bromhal, G.S., Strazisar, B.R., Wells, A.W., 2011. Probabilistic design of a near-surface CO_2 leak detection system *Environ. Sci. Technol.* **45**(15), 6380–6387.

Zhang, Y., Vouzisb, P., Sahinidis, N.V., 2011. GPU simulations for risk assessment in CO_2 geologic sequestration, *Comput. Chem. Eng.*, **35**, 1631–1644.

Zhou, Q., Birkholzer, J.T., Tsang C-F., Rutqvist, J.A., 2008. A method for quick assessment of CO_2 storage capacity in closed and semi-closed saline formations, *Int. J. Greenh. Gas Control* **2**, 626–639.

This preprint was prepared with Yunwei Sun's LaTeX macros v4. File global1 formatted August 3, 2012.

Table 3. Sobol' sensitivity indices

	t(y)	R^2	x_{13}	x_{12}	x_{11}	x_{10}	x_9	x_8	x_7	x_6	x_5	x_4	x_3	x_2	x_1
	10	0.9880	0.0000	0.0220	0.0643	**0.8970**	-	0.0637	-	-	-	-	-	-	-
	20	0.9900	0.0000	0.0140	0.0889	*0.7180*	-	0.2230	-	-	-	-	-	-	-
P	50	0.9962	0.0000	0.0050	0.1160	0.2630	-	*0.6480*	-	-	-	-	-	-	-
	80	0.9982	0.0000	0.0023	0.1100	0.1200	-	**0.7970**	-	-	-	-	-	-	-
	100	0.9987	0.0000	0.0017	0.1040	0.0801	-	**0.8380**	-	-	-	-	-	-	-
	10	0.9957	0.0000	0.1180	0.0489	**0.8910**	-	0.0146	-	-	-	-	-	-	-
	20	0.9957	0.0000	0.1240	0.0529	**0.8870**	-	0.0251	-	-	-	-	-	-	-
S_c	50	0.9951	0.0000	0.1210	0.0558	**0.8650**	-	0.0452	-	-	-	-	-	-	-
	80	0.9953	0.0000	0.1180	0.0576	**0.8580**	-	0.0583	-	-	-	-	-	-	-
	100	0.9954	0.0000	0.1140	0.0594	**0.8550**	-	0.0641	-	-	-	-	-	-	-
	10	0.9151	0.1250	0.0233	0.0268	0.1030	**0.9680**	0.1620	-	-	-	-	-	-	-
	20	0.9290	0.0420	0.0185	0.0041	0.0980	**0.9690**	0.1300	-	-	-	-	-	-	-
Q_c	50	0.9451	0.0729	0.0148	0.0111	0.0666	**0.9410**	0.1580	-	-	-	-	-	-	-
	80	0.9535	0.0335	0.0145	0.0060	0.0575	**0.9590**	0.1300	-	-	-	-	-	-	-
	100	0.9569	0.0335	0.0062	0.0054	0.0342	**0.9860**	0.1210	-	-	-	-	-	-	-
	10	0.8012	0.2690	0.1560	0.0478	0.2350	*0.7390*	*0.5550*	-	-	-	-	-	-	-
	20	0.7699	*0.5730*	0.2610	*0.5540*	0.4880	**0.8240**	**0.8520**	-	-	-	-	-	-	-
Q_b	50	0.7281	0.4320	0.1160	**0.8020**	*0.5840*	*0.6910*	**0.7650**	-	-	-	-	-	-	-
	80	0.6962	0.1670	0.1530	0.1450	0.4180	**0.7540**	**0.8020**	-	-	-	-	-	-	-
	100	0.6852	0.4760	0.2160	0.4250	*0.5490*	**0.8870**	**0.9190**	-	-	-	-	-	-	-
	10	0.9425	-	0.0113	0.0000	0.1190	**0.9250**	0.0881	0.0000	0.1650	0.0097	0.0187	0.0000	0.0237	0.0448
	20	0.9496	-	0.0000	0.0087	0.0971	**0.9320**	0.1010	0.0068	0.2490	0.0000	0.0244	0.0035	0.0636	0.1060
U_p	50	0.9425	-	0.0000	0.0000	0.0578	**0.8780**	0.1300	0.0000	0.2230	0.0604	0.0671	0.0284	0.0245	0.0708
	80	0.9487	-	0.0000	0.0051	0.1870	**0.8920**	0.2220	0.0048	0.1640	0.0616	0.1350	0.0000	0.0395	0.0400
	100	0.9503	-	0.0336	0.0000	0.0674	**0.8990**	0.1160	0.0000	0.3570	0.0481	0.0973	0.0081	0.0387	0.0724
	10	0.7719	-	0.0229	*0.5490*	0.0444	**0.8550**	0.4340	0.0345	0.0238	0.0193	*0.6130*	0.1500	0.0078	0.1270
	20	0.7870	-	0.1120	0.0000	**0.8480**	0.1630	0.3040	0.0219	0.0000	0.2050	0.3640	0.0467	0.1110	0.1180
U_t	50	0.6764	-	0.0000	0.0204	0.0396	*0.5280*	0.0767	0.4100	0.0079	0.0000	1.0300	0.0000	0.2850	0.0281
	80	0.6513	-	0.0490	0.4640	0.1850	0.2960	*0.6340*	*0.5430*	0.2240	0.2200	0.2540	0.1060	0.2410	0.1030
	100	0.7642	-	0.1440	0.3050	0.2860	0.0247	0.0160	0.1140	0.0390	0.4390	0.3200	*0.6400*	0.1170	0.1970

Inputs: x_1: sand volume fraction; x_2: correlation length in x; x_3: correlation length in z; x_4: sand permeability; x_5: clay permeability; x_6: fault length in x; x_7: brine molality; x_8: caprock permeability; x_9: fault permeability; x_{10}: reservoir permeability; x_{11}: injection rate; x_{12}: fault-injector distance; x_{13}: Lumped aquifer permeability

Outputs: P: reservoir pressure at fault inlet; S_c: CO_2 saturation at fault inlet; Q_c: CO_2 leakage rate at fault outlet; Q_b: brine leakage rate at fault outlet; U_p: impacted volume for pH < 6.5; U_t: impacted volume for TDS > 1500 mg L^{-1}

The dashes in the table indicate irrelevant inputs.

Sobol's sensitivity indices are classified as (1) very important ($>$ **0.75**), (2) important (*0.5*∼*0.75*), (3) insignificant (0.2∼0.5), and (4) irrelevant ($<$ 0.2).